The Effect of the Cleaning and Repainting on Ship Drag Penalty

I K A P Utama
Department of Naval Architecture, Institut Teknologi Sepuluh Nopember, Surabaya, Indonesia
kutama@na.its.ac.id

B Nugroho*
Department of Mechanical Engineering, the University of Melbourne, Melbourne, Australia
* Corresponding author: bagus.nugroho@unimelb.edu.au

M Yusuf
PT Dharma Lautan Utama, Surabaya, Indonesia
yusufme93@gmail.com

F A Prasetyo
PT Biro Klasifikasi Indonesia, Jakarta, Indonesia
fredhiagung@bki.co.id

M L Hakim
Department of Naval Architecture, Institut Teknologi Sepuluh Nopember, Surabaya, Indonesia
mluqmanhak@gmail.com

I K Suastika
Department of Naval Architecture, Institut Teknologi Sepuluh Nopember, Surabaya, Indonesia
k_suastika@na.its.ac.id

B Ganapathisubramani
Aerodynamics and Flight Mechanics Research Group, University of Southampton, Southampton, the United Kingdom
G.Bharath@soton.ac.uk

N Hutchins
Department of Mechanical Engineering, the University of Melbourne, Melbourne, Australia
nhu@unimelb.edu.au

J P Monty
Department of Mechanical Engineering, the University of Melbourne, Melbourne, Australia
montyjp@unimelb.edu.au

Abstract

Although the hull of a recently dry-docked large ship is expected to be relatively smooth, the surface scanning and experiment reveals that it can exhibit an "orange-peel" roughness pattern with an equivalent sand-grain roughness height $\boldsymbol{k_s}$ **= 0. 101 mm.** Using the known k_s value and integral boundary layer evolution, a recently cleaned and coated full-scale ship is predicted to experience a significant increase in the average coefficient of friction $\%\Delta\bar{C}_f$ and total hydrodynamic resistance $\%\Delta\bar{R}_T$ during operation. Here the report also discuss two recently reported empirical estimations **(**Chan et al. J. Fluid Mech (2015), 771, 743–777 and Forooghi et al. J. Fluids Eng (2017). 139(12): 121201 **)** that can estimate k_s directly from measured surface topographical parameters, by-passing the need for experiments on replicated surfaces. The empirical estimations are found to have an accuracy of 4.5 – 5 percentage points in $\%\Delta\bar{C}_f$.

Keywords: turbulent boundary layer; skin friction drag; ship-hull roughness; roughness estimation.

Introduction

It is estimated that there are more than 100,000 ships operating worldwide, consuming around 200-300 million metric tons of fuel per year, resulting in a significant economic and environmental impact (Cobert et al. 1999; Winebrake et al. 2009). In the last few decades, there have been various efforts by industry to mitigate fuel consumption of ships, including improved propulsion system design, additional renewable energy sources such as implementing solar panels, and better hull design (see Molland et al. 2014 for recent reviews). Although these developments are beneficial, naval architects must also consider the contribution to fuel consumption of skin friction drag over the hull surface, which is particularly significant for large ships. For large marine vehicles, such as very large crude carriers (VLCC), around 80% of the total drag experienced by the vessel is due to skin friction drag (Kodama et al. 2000).

Skin friction drag on ship hulls arises from the turbulent boundary layers (TBL) that form over the hull. An important parameter in describing turbulent flow is Reynolds number, $Re = U_\infty L/v$, where U_∞ is freestream mean velocity (steaming speed), L is characteristic length scale (usually the boundary layer thickness δ or ship length), and v is kinematic viscosity of the fluid. For wall-bounded flow, it is instructive to define the Friction Reynolds number $Re_\tau = U_\tau \delta/v$, where U_τ is skin friction velocity given by $U_\tau = \sqrt{\tau_w/\rho}$ where τ_w is wall shear stress and ρ is fluid density. The friction velocity, U_τ, can be used to calculate the local coefficient of friction, $C_f = 2(U_\tau/U_\infty)^2$.

The already high skin friction drag on ship hulls due to TBLs is exacerbated if the hull surface is rough. Hull roughness on an operating ship is a major issue in the shipping industry, as it is known to cause additional ship drag penalty, leading to an increase in the powering requirement and fuel usage (Lackenby 1962; Townsin et al. 1981; Townsin 2003; Schultz. 2007; Schultz et al. 2011). This roughness is generally in the form of biofouling and hull imperfections due to repeated cleaning (scraping, water blasting,

sandblasting) and application of anti-corrosion and anti-fouling coatings. There have been many efforts in the last few decades at estimating the drag penalty due to roughness by scaling of smaller-scale turbulent boundary layer predictions to full-scale ships (Granville 1958; Grigson 1985;1987, Schultz 2007; Monty et al. 2016; Pullin et a. 2017). Such methods rely on the universality of the mean velocity profiles (Townsend 1976; Marusic et al. 2013), where the viscous scaled mean velocity profile U^+ (where $U^+ = U/U_\tau$) over a rough surface is assumed to be similar to that of a smooth surface, but with an additional downward shift ΔU^+, referred to as the Hama (1954) roughness function, representative of an increase in wall drag. The shift ΔU^+ is a function of the viscous scaled roughness height. To permit comparisons across different roughness geometries, ΔU^+ is typically defined in terms of k_s, the equivalent sandgrain roughness, derived from the studies conducted by Nikuradse (1933). k_s, which equates a given roughness to a hypothetical surface composed of close-packed uniform sand grains is not a geometric height, but a measure of the surface roughness effect on the turbulent boundary layer. Unlike topographical parameters that can be physically measured, the equivalent sand-grain roughness height k_s can only be obtained by exposing the surface roughness of interest to a flow, either experimentally or within simulations (Hama 1954; Perry and Joubert 1963; Perry et al. 1969; Thakkar et al. 2018). At sufficiently high Reynolds number, the pressure drag-component over roughness elements dominates over the viscous component. This situation manifests in the log-linear relationship between $\Delta U^+$and k_s^+ and is generally termed "fully-rough" flow (Nikuradse 1933). Note however, not all surface roughness can be quantified with ΔU^+ and k_s. Roughness patterns that have a correlation between ΔU^+ and k_s are generally called the *'k-type'* roughness category, while those that do not are termed *'d-type'* (see Perry and Joubert 1963; Perry et al. 1969). Many ship hull imperfections and biofouled surfaces tend to fall into *'k-type'* category, hence it is possible to characterize them by ascribing an equivalent sand-grain roughness.

Obtaining U_τ, ΔU^+, and k_s allows one to extrapolate laboratory (or numerical) results to a full-scale ship and estimate the drag penalty via mean momentum integral methods, which was first described by Prandtl and Schlichting (1955), followed by Granville (1958). A key assumption in this extrapolation is Townsend's (1976) outer layer similarity hypothesis which postulates that at a sufficiently high Reynolds number, beyond the surface roughness sublayer region, turbulent motions are independent of the surface roughness and viscosity. This hypothesis has been the subject of many studies (see Jimenez 2004; Schultz and Flack 2005; 2007; Flack et al. 2005, 2007; Wu and Christensen 2007; Monty et al. 2011, 2016). A critical aspect of Townsend's outer layer similarity hypothesis is that boundary layer thickness δ has to be sufficiently larger than the roughness height, i.e. $\delta/k \geq 40$ (Jimenez 2004). Any roughness that substantially relaxes this ratio (larger k and smaller δ), could have a severely curtailed logarithmic region, and the flow may behave more like flow over obstacles, than a TBL formed over a rough surface.

Although a combination of experiment and mean momentum integral methods can produce a drag approximation for a full-scale ship (see Granville (1958), Schultz (2007), Monty et al. (2016) and Pullin et al. (2017)), the Achilles heel of this process is

the experimental (or numerical) cost of determining k_s (a required step in the procedure). Due to this, many marine engineers rely on various empirical estimations (Townsin et al. 1980; 1981, Townsin 2003). However, many of the available methods lack accuracy due to the inability to reduce the complex interaction between a surface and the TBL down to simple geometric parameters. A recent report by Chan et al. (2015) showed that one would need a minimum of two easily obtained roughness parameters, namely average roughness height and effective slope to estimate the increase of drag penalty in a wall bounded flow due to an irregular surface. Other studies have suggested that skewness is also a key parameter (Flack and Schultz 2010; Forooghi et al. 2017).

Intuitively, it might be expected that the hull of a recently cleaned and painted ship would be smooth. However, from a hydrodynamic perspective, this is not necessarily the case and depends very much on flow conditions (Schultz 2002; 2004; 2007). The near-wall fluid flow will become altered once the roughness height becomes approximately equivalent to the viscous length scale ν/U_τ. Schultz (2004) conducted experiments to measure the drag penalty on a "cleaned" surface. The "clean" surface was a previously fouled flat plate with the fouling removed using a nylon brush. The cleaned surface experiences a drag penalty increase of 3% - 15% over a hydrodynamically smooth plate. Note that Schultz (2004) uses a new surface plate for his cleaned surface case, which may have a better surface compared with an actual ship hull that has been exposed to repeated scraping, sand blasting, water blasting, and painting over its service life.

This study aims to obtain the equivalent sand-grain roughness height k_s of a recently cleaned and painted ship hull. The methods of investigation are similar to that of Monty et al. (2016), where the steps are : (1) to conduct an imprint of the hull roughness using silicone rubber, (2) to manufacture a scaled roughness for wind-tunnel experiments, (3) to conduct boundary layer measurements using hot-wire anemometry to obtain the equivalent sand-grain roughness height k_s, (4) to use the result to estimate the corresponding roughness-related drag penalty on full-scale operating ships, following the method of Prandtl and Schlichting (1955) and Granville (1958). Finally, this report will also compare the experimentally measured k_s with the recently reported empirical estimation technique of Chan et al. (2015) and Forooghi et al. (2017).

Materials and Methods

Ship Details

The ship test bed is a Ro-Ro ferry (the Dharma Kencana IX) owned and operated by PT Dharma Lautan Utama (Figure 1). The company is one of the largest and the best passenger ship operators in Indonesia. The well-known company pride itself in its high-quality service, safety, and staff professionalism. In term of awards and recognition, PT Dharma Lautan Utama comes second, only to the country's national aircraft carrier, which in itself illustrate the company's high performance. The well-maintained Dharma Kencana IX ferry was built in the late 1980's and has an overall length (LOA) of 71.82 m with a predominantly flat bottom, and waterline length (L.W.L) of 68.46 meter. The ship operates daily serving the Merak-Bakauheni route in Sunda Strait, Indonesia, the busiest route in Indonesia connecting the island of Sumatera and Java. It has a cruising

velocity of around 9-10 knots, which translates to approximately 4.5 – 5 m/s. The ferry has the ability to go faster, however due to the high passenger and ferry volume between the two ports, such practice would cause a bottleneck at the ports (see Nugroho et al. 2017 to view the average velocity record for ships operating in this route).

Figure 1 : Dharma Kencana IX ferry from PT Dharma Lautan Utama (PT DLU)

The Indonesian regulator requires all Indonesian flagged or International flagged Ro-Ro ferries that operate in Indonesian waters to conduct dry-docking annually. Hence, once every 11-12 months, this ship hull would be assessed and cleaned. The cleaning activities depend on the severity of the hull condition and how thick the left-over coating was. For example, if the ship hull is covered by thin slime and the coating thickness is deemed acceptable until the next scheduled dry-docking, cleaning would be limited to water pressure-hosing only. If there are a few small spots where biofouling starts to grow, those particular locations will be scraped, water-hosed, spot/sand blasted and re-coated with anti-fouling paint. From the authors observation, PT Dharma Lautan Utama's fleet tend to receive a more thorough hull cleaning and maintenance than the other smaller and less well-known ship operators in the area. For this study case, the Dharma Kencana IX ship hull was scraped, water pressure-hosed, and spot blasted to remove the old anti fouling paint. Sand-blasting to bare steel was not conducted. The hull is then painted with corrosion-resistant coatings (Hempadur 47182) and epoxy primer (Hempadur Quatro 17634). Finally, a low friction, self-polishing antifouling copolymer (SPC) Hempel A/F Globic 9000 was applied. The painting of the hull were conducted in the morning until late afternoon where the average temperature was around 30^{o} – 33^{o} Celsius with average humidity of 75%.

Surface Roughness Pattern

Surface roughness imprint and scanning

The surface roughness pattern from a recently cleaned and painted ship hull is obtained by using an imprint of silicone rubber during dry-docking (Figure 2c). The roughness sample was taken from the flat bottom, around 25 m downstream of the bow. The imprint used here is Extrude-Wash (light body) from Kerr™ which is typically used for dental imprints. The imprint is later scanned using a Keyence™ LK-031 laser triangulation sensor that is attached to a high-precision two-axis computer-controlled positioning system. The laser scanner has a horizontal (x and y) resolution of 30 µm and a vertical resolution (z) of 1 µm. The horizontal scanning covers a surface area of 50 x 50 mm. Figure 2a and 2b show the scanned roughness topography and the associated probability distribution function (p.d.f) of the surface elevation z respectively.

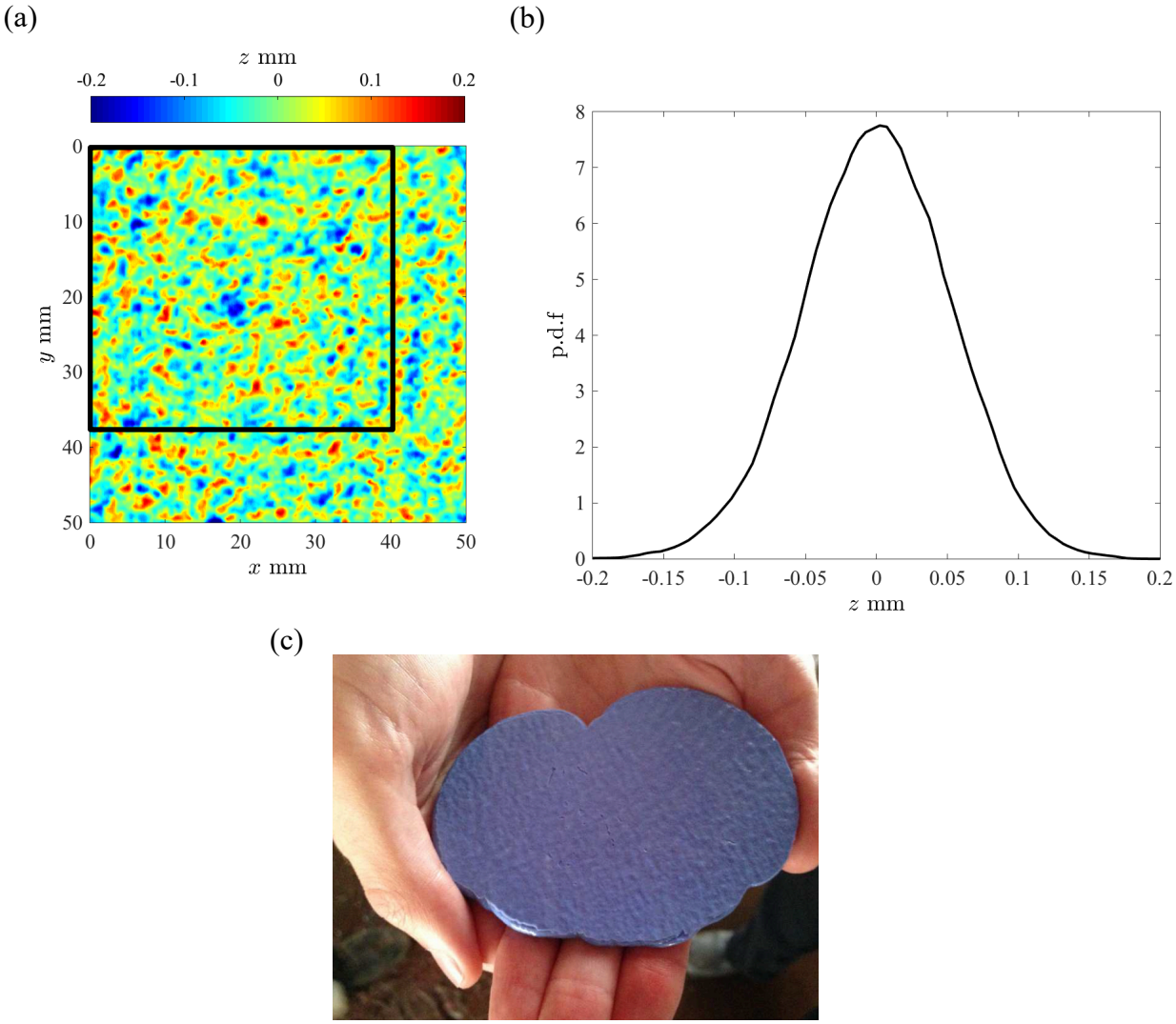

Figure 2. Details of the surface roughness scan. (a) contour map of the surface topography, (b) shows the p.d.f of the surface roughness height, and (c) the original imprint from the flat underside of the ship hull. The solid black line on the original

roughness scan (figure a) represents the periodic sub-area used to construct the 2.5× scaled roughness plate.

The important roughness parameters such as average roughness height k_a and root-mean-square height k_{rms}, are tabulated in Table 1, along with definitions (here z' is the deviation of the roughness elevation about the mean). In the shipping industry, the average peak-to-trough roughness height over a 50 mm fetch of the surface ($R_t(50)$) is often used as a roughness length scale (see Townsin et al. 1980; 1981; Townsin 2003). In this roughness case, the imprint and surface scanner yields $R_t(50)$ = 0.264 mm. Schultz (2007) defines $R_t(50)$ = 0.15 mm as a 'typical as applied anti fouling' and $R_t(50)$ = 0.3 mm as 'deteriorated coating', hence the roughness lies between those two states (although closer to the latter). This may be due to the lack of sandblasting down to the bare steel during dry-docking, or due to the conditions during application: high temperature (30° - 33° Celcius) and humidity (75%). From personal communication with dry-dock operators, the ship owner representatives and paint manufacturer representatives, such hull-roughness is common for a recently cleaned and painted ship hull. Even more severe hull roughness conditions are reportedly found on a regular basis on other out-docking ships.

Roughness Parameter	Value	Units	Equation
k_a	0.041	mm	$\overline{\lvert z' \rvert}$
k_{rms}	0.052	mm	$\sqrt{\overline{z'^2}}$
k_p	0.48	mm	$\max z' - \min z'$
k_{sk}	0.087	-	$\overline{z'^3 / k_{rms}^3}$
k_{ku}	3.071	-	$\overline{z'^4 / k_{rms}^4}$
ES_x	0.089	-	$\overline{\lvert dz'/dx \rvert}$
$R_t(50)$	0.264	mm	

Table 1: Topographical parameters of the unscaled roughness.

Surface roughness tile manufacturing

The scanned roughness topography is scaled by a factor of 2.5 in the *x*, *y* and *z* directions. This scaling value is chosen to nominally capture ship operating conditions at the highest speed of the available facility. It is necessary to attain fully rough conditions in the experiments to obtain the equivalent roughness height k_s, although it is not possible *a-priori* to guarantee whether this will be the case. Over-scaling the surface, though tempting in terms of assuring fully rough conditions, has the disadvantage of reducing δ/k which may result in the surface behaving as an obstruction rather than surface

roughness. The average roughness height parameters (i.e k_a) is approximately half of those tested by Monty et al. (2016) (where they have $k_a = 0.094$ mm).

Figure 2a shows the roughness topography and the sub-area (illustrated by black lines, sized 40.4 × 38 mm) that is used to construct the 2.5× roughness plate (Figure 3). The isolated sub-area is uniformly scaled by 2.5× in all three dimensions, resulting in a 101 × 95 mm surface area. To ensure that surface periodicity and tessellation in both spanwise and streamwise directions are obtained, a blended interpolation at the perimeter of the subset is applied. The scaled 101 × 95 mm surface area is then replicated three times in the spanwise direction and five times in the streamwise direction, resulting in a final tile size of 505 x 285 mm (Figure 3). The manufacturing method is similar to that of Nugroho et al. (2013, 2014, 2021) and Monty et al. (2016). The initial blended interpolation arrangement would prevent any unwanted secondary flows that could arise from a surface discontinuity. To manufacture the surface, a master tile made of engineering wax is then machined using a three-axis CNC router. A platinum cured rubber mould is then applied on to the master tile to generate the negative surface roughness pattern. Finally, a series of multiple polyurethane cast/copies of the original master tile can be made. To ensure strong structural integrity, the polyurethane is mixed with aluminium powder. In total, 30 tiles are produced, forming a 5.05 x 0.855 m^2 test surface in the entire wind tunnel working section.

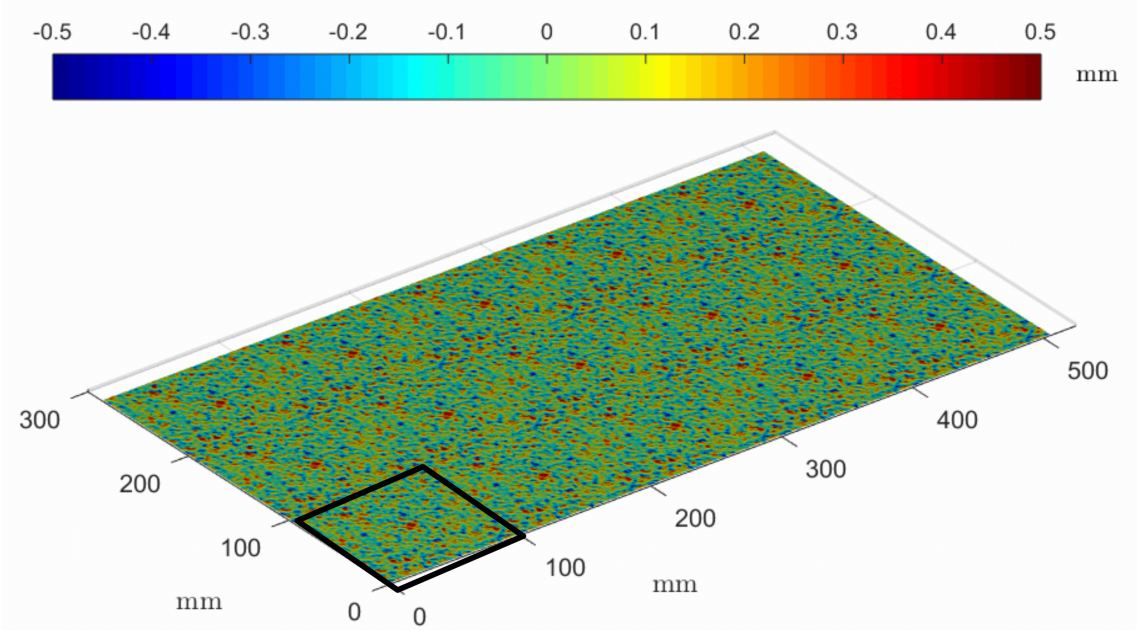

Figure 3: Surface roughness geometry scaled by a factor of 2.5 with tile size 505 x 285 mm.

Experiment Facility

Wind tunnel

The experiments are performed in a boundary layer wind tunnel at the University of Melbourne. The wind tunnel is an open-return blower type with a contraction area ratio

of 8.9:1, and settling chamber featuring a honeycomb and five mesh screens. The wind tunnel working section has a cross-section area of 0.94 x 0.375 m (width × height) with a streamwise length of 6.7 m. The inlet of the working section has a 100 mm long strip of P40 sandpaper that acts as a trip to ensure a repeatable and well-defined transition from laminar to turbulent flow (following the study of Marusic et al. 2015; 2016). To ensure a seamless interchange between the smooth and rough surface, the steel plate covered test section floor can be lowered using hydraulic lifts. Figure 4 shows the wind tunnel experimental set-up with the roughness plates in-place.

Figure 4 : Wind tunnel experiment set-up with roughness plates in-place.

Hot-wire anemometer

The flow measurements were performed using an in-house-built Melbourne University Constant Temperature Anemometer (MUCTA) system (see Perry (1982) and Perry and Morrison (1971) for MUCTA details). The hot-wire probe used is a single-normal hot-wire probe (*Dantec type 55P05*) that is connected to a 4 mm diameter probe support (*Dantec type 55H21*). For the sensing element, a 5 μm Platinum Wollaston wire is used, and to minimise attenuation due to end conduction it is etched with a length of 1 mm, resulting in a length-to-diameter ratio $l/d \approx 200$ (Ligrani and Bradshaw 1987; Hutchins et al. 2009). Because measurements are conducted with the same hot-wire across a range of freestream velocities (to obtain various Reynolds number), the viscous scaled wire length l^+ (where $l^+ = l\,U_\tau/\nu$) will vary in the range $25 < l^+ < 71$. Thus, at the higher velocity the measurements will experience attenuation due to insufficient

spatial resolution (Ligrani and Bradshaw 1987; Hutchins et al. 2009). The hot-wire is calibrated in-situ in the freestream before and after each measurement. To minimise error due to hot-wire drift, a correction is conducted by periodically moving the hot-wire to the freestream which provides a single recalibration point that can be used to adjust the calibration (Talluru et al. 2014). The hot-wire probe is attached to a two-dimensional computer controlled traversing system, which permit measurements over a spanwise and wall-normal plane.

Aerodynamic Measurement

Experiment conditions

In this study, x, y, and z represent the streamwise, spanwise, and wall-normal directions, with u, v, and w representing the corresponding velocity components. The upper-case velocity components U, V, and W represent time averaged or mean values. Here superscript + represents viscous scaling for velocities $U^+ = U/U_\tau$ and wall normal distance $z^+ = z\,U_\tau/\nu$. The boundary layer thickness δ is defined as the wall normal position where the mean velocity U recovers 98% of the freestream velocity U_∞.

Measurement cases

Two measurements are made, one above the smooth wall reference and the second above the rough surface (refer to Table 2 for key flow parameters). For the smooth wall case, the flow measurement is performed at the downstream location of $x = 4$ m at nominal velocity 15 m/s. The hot-wire measures the streamwise velocity profile at 50 logarithmically spaced measurement points in the wall-normal direction covering 150 mm overall traverse height ($\approx 3\delta$). Data are sampled using a Data Translations DT9836 16 bit analogue digital converter with a sample duration of 150 s and acquisition frequency of 50 kHz, corresponding to a boundary layer turn over time $\approx 45{,}000\delta/U_\infty$.

Surface type	U_∞ (m/s)	x (m)	δ (m)	U_τ (m/s)	C_f $(2(U_\tau/U_\infty)^2)$	Re_τ	ΔU^+	l^+
Smooth	14.90	4	0.050	0.55	2.73×10^{-3}	1800	-	37
Rough	10.21	4	0.060	0.39	2.92×10^{-3}	1500	0.59	26
Rough	15.13	4	0.058	0.59	3.04×10^{-3}	2200	1.50	39
Rough	20.20	4	0.059	0.78	2.98×10^{-3}	3000	2.01	52
Rough	25.27	4	0.061	0.99	3.07×10^{-3}	3900	2.83	66
Rough	28.66	4	0.063	1.12	3.05×10^{-3}	4460	3.09	71

Table 2. Key flow parameters

For the rough wall case, the measurements are also conducted at the downstream location $x = 4$ m, at four different nominal velocities (10 m/s, 15 m/s, 20 m/s, 25 and 28 m/s). For all rough wall cases, a two-dimensional flow mapping was performed, where the hot wire is traversed over a 31 logarithmically spaced points in the wall-normal direction and 11 linearly spaced points in the spanwise direction which measures 150 ×

150 mm ($\approx 2\delta \times 2\delta$). The total sample duration at each measurement points are reduced to 30 s at 50 kHz to minimise drift over the 341 individual measurements. The measurements correspond to a boundary layer turn over time $\approx 4{,}000\delta/U_\infty$ to $12{,}500\delta/U_\infty$ (from the lowest to the highest velocities), and a viscous scaled sample interval $\Delta t^+ < 1.3$. The reason why two-dimensional flow mappings were conducted, is because the current surface roughness is a naturally occurred type roughness, which may have different mean streamwise velocity profiles in the spanwise direction. This way, it could capture more of the flow dynamics.

Estimating skin friction velocity U_τ , ΔU^+ , and k_s

The skin friction velocity U_τ over the smooth wall can be estimated using the Clauser (1954, 1956) technique by fitting the measured mean velocity profile onto the log-law:

$$U^+ = \frac{U}{U_\tau} = \frac{1}{\kappa} log\left(\frac{z\,U_\tau}{\nu}\right) + A, \tag{1}$$

where Kármán constant $\kappa = 0.39$ and the smooth wall intercept $A = 4.3$ (see Marusic et al. 2013). For the rough wall case, traditionally one would employ the modified Clauser method, by fitting the mean velocity profile on to a modified log-law:

$$U^+ = \frac{U}{U_\tau} = \frac{1}{\kappa} log\left(\frac{(z+e)\,U_\tau}{\nu}\right) + A - \frac{\Delta U}{U_\tau}. \tag{2}$$

However, The introduction of the rough surface results in two additional unknowns, namely the roughness offset e and Hama roughness function ΔU^+ or $\Delta U/U_\tau$ (Hama 1954; Perry and Joubert 1963; Perry et al. 1969). In this study, for simplicity e is defined as the median height of the roughness as it provides the optimum fitting in the log-region. The value of e depends on the fluid flow and the roughness elements. Obtaining an accurate value of e experimentally is difficult. One common method of determining e is by iteration on the modified Clauser method (Perry and Joubert 1963; Perry et al. 1969; Perry and Li 1990; Schultz and Flack 2005). Other methods include using a combination of mean velocity-defect and displacement thickness (Furuya et al. 1976; Bandyopadhyay 1987), and assuming that e is half of the roughness height, $k/2$ (Squire et al. 2016b; 2016a; Morrill-Winter et al. 2017). ΔU^+ indicates the change in skin-friction velocity due to the surface imperfection, where a vertical shift upwards indicates a decrease in skin friction drag, while a vertical shift downwards translates to an increase in skin friction drag. Estimating ΔU^+ accurately via the modified Clauser method is notoriously challenging due to uncertainty in determining the limit of the log-region and the wall-normal distance (particularly in determining the initial position of the hot-wire above the uneven surface due to the unknown roughness offset e). Schultz (2004) estimates that the experimental uncertainty in estimating ΔU^+ varies between 6% -16%. In term of k_s, it would lead to 10% - 27% uncertainty.

Due to the combination of these factors, for the rough wall cases, the skin friction velocity U_τ for each free stream velocity cases are obtained by spanwise averaged the 11 mean velocity profiles followed by forcing the outer layer similarity in the velocity defect and outer scaled turbulence intensity. This technique is proposed by Monty et al. (2011) where Townsend's (1976) outer layer similarity hypothesis is assumed to be valid in both the mean velocity and variance profiles. The correctly obtained U_τ value is assumed to be that which best collapses both the mean velocity defect profile and turbulence intensity (scaled with U_τ and δ). The assumed outer layer similarity method of Monty et al. (2011) is also compared with the more traditional method, using the modified Clauser technique. The U_τ values obtained from both methods agree to within 9%. A similar method is also conducted by Ramani et al. (2020) and Nugroho et al. (2018, 2021)

Using outer layer similarity method of Monty et al. (2011), one would obtain U_τ and ΔU^+ that can be used to obtain the equivalent sand-grain roughness height k_s by fitting the ΔU^+ onto the fully rough asymptote :

$$\Delta U^+ = \frac{\Delta U}{U_\tau} = \frac{1}{\kappa}\ln\left(\frac{k_s U_\tau}{\nu}\right) + A - B \tag{3}$$

where B is typically 8.5 (taken from Nikuradse (1933)).

Results and Discussion

Figure 5 shows the turbulent flow statistics for the smooth wall case (solid line) and the rough wall case (open symbol). Figure 5a shows the inner-scaled mean velocity profile where there is a clear vertical shift down, ΔU^+, for the rough wall cases (relative to the smooth wall case) which increases with increasing Reynolds number. For the rough wall case, Figure 5(b) shows an increase in turbulence activity further from the wall, indicated by the vertical shift up of turbulence intensity, particularly at the logarithmic and outer region. However, this is purely the effect of increasing Reynolds number. Figure 5(c) and (d) show the mean velocity-defect profile and outer scaled turbulence intensity respectively. In this form, the two plots clearly show the collapse of the rough walled profiles onto the smooth wall reference case, supporting Townsend's (1976) outer layer similarity hypothesis. The mean velocity-defect (Figure 5c) is described in terms of outer scaling by:

$$U^+_{def} = \frac{U_\infty - U}{U_\tau} = -\frac{1}{\kappa} log\left(\frac{z}{\delta}\right) + C \tag{4}$$

where the intercept C = 3.0 was found via least-square-error fit on the rough and smooth wall data (Monty et al. 2011).

To ensure that the experiments have achieved a fully rough regime, where the local skin friction becomes constant at a sufficiently high Reynolds number (Jimenez 2004; Schultz et al. 2005; Monty et al. 2016), the local coefficient of friction C_f is calculated and tabulated in Table 2. The results show that at nominal free stream velocity 10 – 28 m/s, the C_f values are $\approx 2.92 \times 10^{-3} - 3.07 \times 10^{-3}$ (less than 5% variations

between the lowest and highest Reynolds number), suggesting that to the accuracy that the analysis can determine U_τ, the flow has reached the fully rough condition.

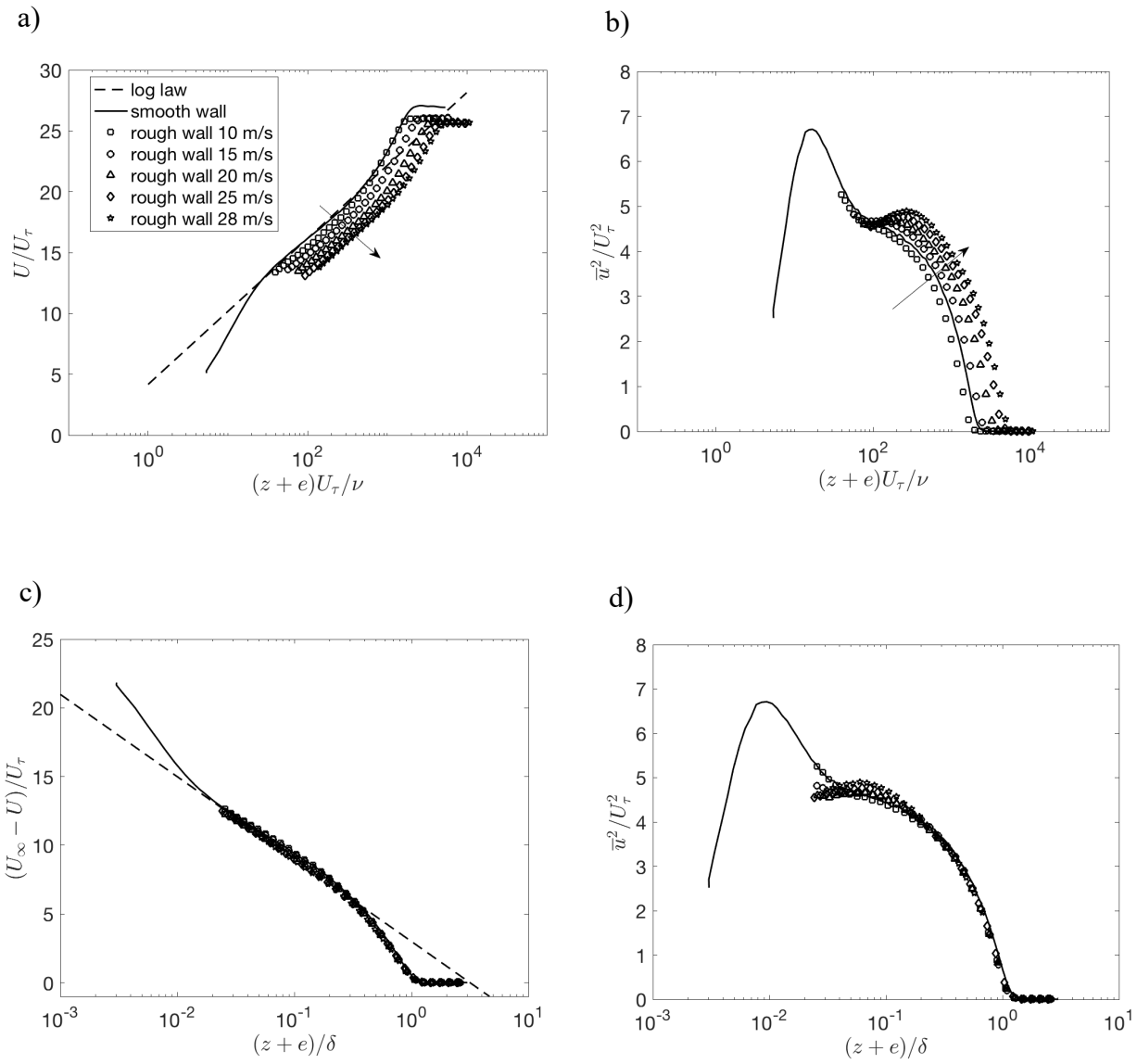

Figure 5: Wall-normal profiles of: (a) inner-scaled mean velocity profile; (b) inner-scaled turbulence intensity; (c) mean velocity-defect; (d) outer-scaled turbulence intensity. The solid lines indicate the smooth wall reference case, and the dashed lines in figure a follow the smooth wall log-law (Equation 1) and c follow the mean velocity defect (Equation 4). Open symbols are rough surface data for the 2.5× scaled roughness with: U_∞ = 10 m/s, squares; U_∞ = 15 m/s, circles; U_∞ = 20 m/s, triangles; U_∞ = 25 m/s, diamonds; U_∞ = 28 m/s, pentagram.

The resulting Hama roughness function ΔU^+ is then plotted against the viscous scaled equivalent sand-grain roughness height k_s^+, by fitting ΔU^+values onto the fully rough asymptote (Figure 6). This results in an equivalent sand-grain roughness value of

0.253 mm for the scaled surface tested in the wind tunnel. From the figure, it is clear that the flow behaviour is different from the standard Colebrook-type (Colebrook and White 1937) roughness (dot-dashed line) and the sparse biofouled surface investigated by Monty et al. (2016) (solid line). The flow seems to exhibit a fully-rough behaviour even from a low ΔU^+ by collapsing relatively well onto Nikuradse's fully rough asymptote. A similar trend has been reported by Shockling (2006); Schultz and Flack (2007); Schultz et al. (2015); and Flack et al. (2016) where their Hama roughness functions collapse well with Nikuradse's fully rough asymptote at $\Delta U^+ < 4$. By applying the factor 2.5 and assuming Reynolds number similarity, the actual k_s value for the recently cleaned ship hull is found to be **0.101 mm**. Thus the k_s value lies around deteriorated coating or light slime rating as reported by Schultz (2007).

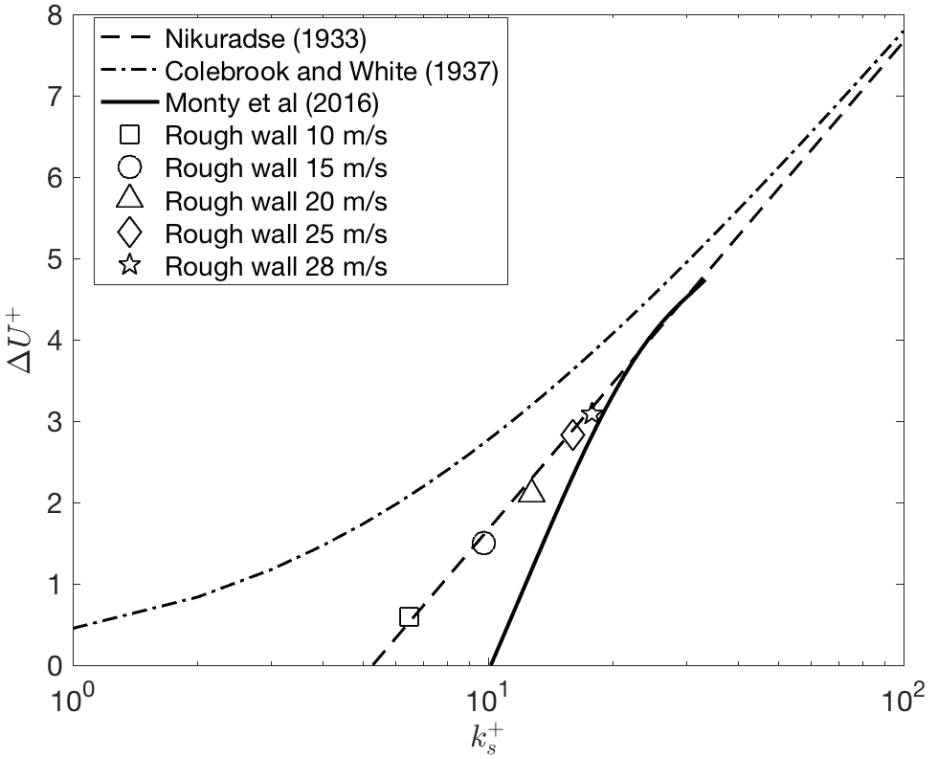

Figure 6: Velocity profile shift (Hama roughness function) as a function of viscous scaled equivalent sand-grain roughness height k_s. Open symbols are the rough surface data with U_∞ = 10 m/s, squares; U_∞ = 15 m/s, circles; U_∞ = 20 m/s, triangles; U_∞ = 25 m/s, diamonds; U_∞ = 28 m/s, pentagram. The dashed line is Equation 3 from Nikuradse (1933), dot-dashed line is from Colebrook and White (1937), solid line is from the sparse biofouled surface tested by Monty et al. (2016).

The results from this experiment are slightly different to those previously reported for a recently cleaned and painted ship hull. Schultz (2004, 2007) report that a typical new protection coating would have a k_s value closer to 0.03 mm (an approximate factor of 3.4 less than the value found in this study). This discrepancy may be due to the fact that the Dharma Kencana ship hull has underlying roughness that accumulated from

multiple cleaning activities over its operational lifetime (scraping, water- and sand-blasting, etc). In addition, for the current study it is likely that the orange peel coating defects have arisen from sub-optimal quality of paint application which may relate to unfavourable conditions in the dry-dock facility (high humidity, high temperature). Other lab-based experiments in the literature assume or use a clean and new steel surface that may have a considerably lower initial roughness, hence yielding a much lower equivalent sand-grain roughness height. A similar situation was reported by Schultz (2004), where a cleaned and painted flat surface (that was previously covered by fouling) would have a higher friction drag than that of a newly-coated surface that had not been fouled. Interestingly however, from a private communication with representatives of the paint manufacturer, the authors are led to believe that the observed hull-roughness is very common for a recently dry-docked ship and it would be classified as an acceptable quality application. Certainly, the authors own observations of dry-docking in Indonesia, have regularly witnessed even more severe roughness on recently cleaned and repainted hulls. Hence, it is concluded that a recently dry-docked, cleaned, and painted ship hull may already have a roughness quality that is similar to that reported previously for deteriorated coating or fouling due to light slime (Schultz, 2007).

Integral boundary layer evolution and full ship scale

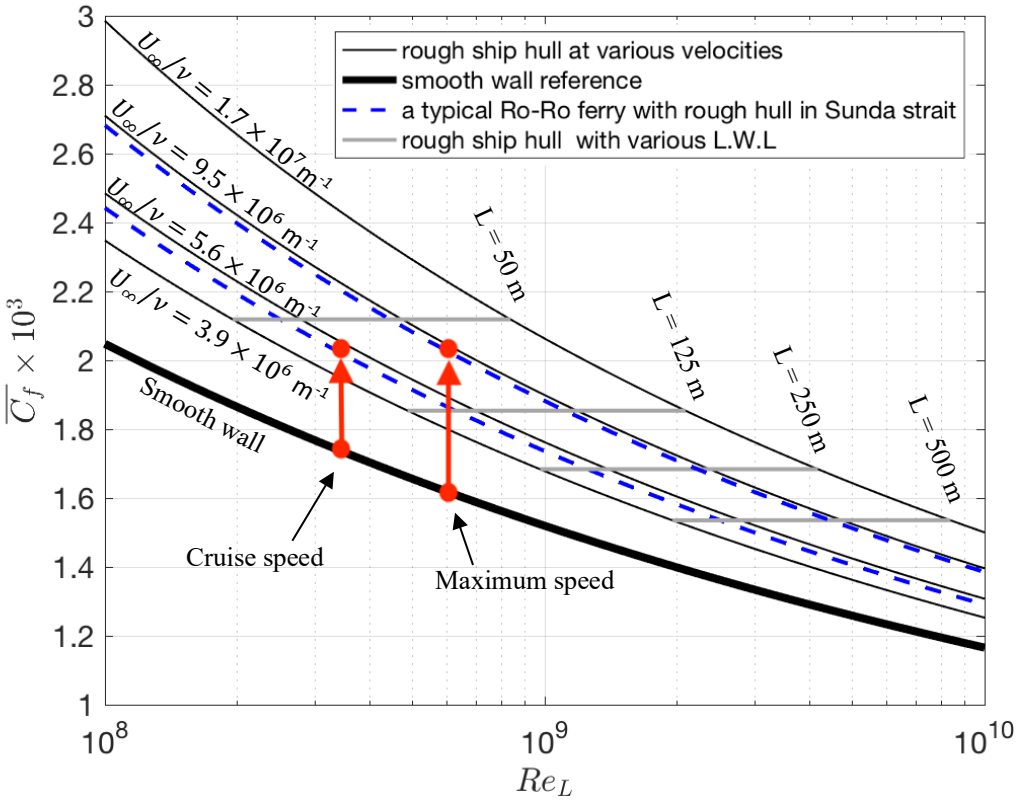

Figure 7 : Average skin friction coefficient $\overline{C_f}$ versus Reynolds number (based on ship length) Re_L for smooth wall (thick black line) and hull roughness from a recently cleaned ship with k_s = 0.101 mm (thin black lines, grey lines and dashed blue lines). The multiple thin black lines represent ranges of ship velocities and the thick grey lines show different

ship lengths. The dashed blue lines show the velocity of a typical Ro-Ro Ferry in Sunda Strait Indonesia (our case) at both cruise velocity (lower blue dashed line) and maximum velocity (higher blue dashed line). The red circle symbols represent the vessel operating points both at cruise and maximum speeds

Assuming the flow behaves as a fully rough flow, the k_s value of 0.101 mm can be used to estimate the drag penalty of a full-scale ship, by assuming a functional form for the viscous scaled mean velocity profile and using a mean momentum integral equation for an evolving Zero-Pressure-Gradient (ZPG) turbulent boundary layer. This study follows the method of Monty et al (2016) and readers are referred to that study for a detailed step-by-step outline of the method. A similar algebraic solution is available in Pullin et al. (2017). Based on Figure 6, the authors assume that ΔU^+ is given by Equation (3) for $k_s^+ \geq \exp(\kappa(\mathrm{B}-\mathrm{A}))$ and $\Delta U^+ = 0$ for $k_s^+ \leq \exp(\kappa(\mathrm{B}-\mathrm{A}))$. The results from both smooth and rough wall turbulent boundary layer evolution are shown in Figure 7. Here the thick black line represents a smooth wall, the thin black lines illustrate rough wall flow (k_s= 0.101 mm) for ships at various unit Reynolds number U_∞/ν, and the grey lines show different ship lengths (fixed k_s/L). Note that the 10% - 27% in k_s estimation uncertainty would lead to around 7% - 10% uncertainty in the average skin friction coefficient $\overline{C_f}$.

The ranges of Reynolds numbers based on ship length ($Re_L = U_\infty L/\nu$) are selected to demonstrate the most common parameter space in various marine engineering applications. Similar to Monty et al. (2016), the estimation is limited to the currently considered ranges of vessel length, speed, and seawater viscosity (dependent on seawater temperature), and can only be used as a general guide for the drag penalty associated with the current hull roughness profile. Therefore, using Figure 7, for any ship that has similar hull roughness characteristic as the current case, its drag penalty, economic and energy expenses can be estimated.

Figure 7 also shows the increase in the average coefficient of friction for a Ro-Ro Ferry at both cruise and maximum velocities due to the underlying hull roughness. From this plot, the percentage change in average skin friction coefficient can be calculated as:

$$\%\Delta\bar{C}_f = 100 \times \frac{\bar{C}_{fr} - \bar{C}_{fs}}{\bar{C}_{fs}} \tag{5}$$

where $\bar{C}_{fr}$ is the rough wall coefficient and $\bar{C}_{fs}$ is the smooth wall coefficient (both coefficients are at the ship Re_L, note that the length here is based on the ship's L.W.L). The Ro-Ro Ferry (or other ships that have comparable size and velocity) will experience a 16.4% increase in $\bar{C}_f$ when compared with a hydrodynamically smooth surface at cruise velocity, and approximately 25.2% at maximum velocity (see Table 3). The increase in average coefficient of skin friction is proportional to the roughness Reynolds number $Re_k = U_\infty k/\nu$, hence the full speed case experiences a higher drag penalty. In addition to the percentage increase in the average skin friction coefficient $\%\Delta\bar{C}_f$, the percentage change in total hydrodynamic resistance $\%\Delta\bar{R}_t$ is given by:

$$\%\Delta\bar{R}_T = 100 \times \frac{\bar{C}_{fr} - \bar{C}_{fs}}{\bar{C}_{fs}\left(1+\frac{C_R}{\bar{C}_f}\right)+C_A} \quad (6)$$

where $C_R/\bar{C}_f$ is the ratio of residuary resistance to friction resistance and C_A is the correlation allowance. The two values are obtained using Holtrop analysis (see Holtrop 1977; 1984, Holtrop and Mennen 1978; 1982) based on the ship hull details that the authors obtained from the ship's owner (PT Dharma Lautan Utama) and from the Indonesian Classification Bureau (PT BKI). The change in total hydrodynamic resistance for this type of ship due to hull roughness during cruise is around 8.2% and approximately 7.5% at full speed. The results show the grave challenges faced by the shipping industry in dealing with surface roughness. This indicates that even a recently dry-docked ship that has been cleaned and painted could already suffer from around 7% - 8% higher drag penalty than anticipated.

Ship	L.W.L (m)	Velocity (m/s)	Viscosity (m^2/s)	Re_L	$\frac{C_R}{\bar{C}_f}$	C_A	$\%\Delta\bar{C}_f$	$\%\Delta\bar{R}_T$
Ro-Ro Ferry	68.46	4.5 (cruise speed)	8.97×10^{-7}	3.43×10^{8}	0.65	5.94×10^{-4}	16.4	8.2
Ro-Ro Ferry	68.46	8 (max speed)	8.97×10^{-7}	6.11×10^{8}	2.10	4.44×10^{-4}	25.2	7.5

Table 3 : Full-scale hull roughness penalty results for a typical Ro-Ro ferry.

Empirical estimation

The experiments described here for ascertaining the equivalent sandgrain roughness height k_s and subsequent drag penalty of an observed hull roughness are time-consuming, expensive, and beyond the scope of routine day-to-day procedures. Since the 1970's there have been numerous attempts by the shipping industry to produce a reliable low-order estimation technique. Currently the widely accepted drag penalty/performance prediction method is based on the work of Townsin (ITTC 2014; Townsin et al. 1980; 1981; Townsin 2003):

$$1000(\bar{C}_{fr} - \bar{C}_{fs}) = 44\left[\left(\frac{AHR}{L}\right)^{\frac{1}{3}} - 10Re_L^{-\frac{1}{3}}\right] + 0.125 \quad (7)$$

where L is ship length, Re_L is Reynolds number (based on ship length), and AHR is the Average Hull Roughness based on $R_t(50)$ averaged over the ship hull surface. Although the Townsin estimation technique is widely used, there are questions regarding its accuracy (Grigson 1987; 1992; Flack and Schultz 2010). Particularly because it is based on a simple measure of the roughness height and does not consider other roughness parameters such as skewness and effective slope known to influence drag (Flack and Schultz 2010; Chan et al. 2015; Forooghi et al. 2017). The Townsin estimation can be tested here using the obtained roughness topography and the operating conditions of the full-scale Ro-Ro Ferry. The results show that at cruise and maximum speed, the $\%\Delta\bar{C}_f$

predicted from Equation (7) are 10.75% and 18.35% respectively, as compared to 16.4% and 25.2% respectively obtained from the experiment results.

A recent report by Chan et al. (2015) shows that one would need a minimum of two roughness parameters, average roughness height and effective slope to estimate the increase of drag penalty due to rough surface in the form of,

$$\Delta U^+ = \frac{\Delta U}{U_\tau} = \frac{1}{\kappa} log\left(\frac{k_a\, U_\tau}{v}\right) + \beta \log ES_x + \gamma \tag{8}$$

where β and γ are constants with value 1.12 and 1.47 respectively. A study by Hutchins et al. (2016) demonstrated that this formulation was able to closely predict the increase in drag penalty due to the tubeworm surface tested by Monty et al. (2016). For the cruise speed, Chan et al.'s (2015) formulation predicts $\%\Delta\bar{C}_f$ = 21.1%**,** while at full-speed the prediction gives $\%\Delta\bar{C}_f$ = 30.1%. The results are differing within 4%-5% to the experiment results (see Table 4 for summary). Note however, that the estimation technique still requires further analysis and validation, and it should be treated at this stage as an approximation. The formulation in Equation 8 was developed for a three-dimensional sinusoidal surface which is similar to the orange-peel roughness tested here (both have zero skewness) which may explain the close predictions in this case. Chan et al. (2015) themselves have mentioned that other parameters may need to be considered (i.e. alignment, sparseness etc.). Therefore, questions remain over the general applicability of this formulation. Attempts to refine correlations are ongoing, and several recent studies have suggested that skewness, which is absent from Chan et al.'s (2015) correlation, is a key parameter in determining k_s (Flack and Schultz 2010; Forooghi et al. 2017; Jelly and Busse 2018).

For the current surface, this report also assess the empirical estimation suggested by Forooghi et al. (2017) which includes skewness in its formulation. They propose that equivalent sand-grain roughness can be estimated using,

$$k_s = \bar{k_t}[0.67\, k_{sk}^2 + 0.93\, k_{sk} + 1.3][1.07(1 - e^{-3.5\, ES_x})] \tag{9}$$

where $\bar{k_t}$ is defined as the height difference between the highest peak and valley over a certain subset of a surface, averaged over several subsets. To compute this, the roughness topography (Figure 2a) is divided into a 4×4 subset that yields $\bar{k_t}$ = 0.329 mm (the percentage variation in $\bar{k_t}$ for different subsets ranging from 3 ×3 to 6 ×6 is less than 10%). From equation 9, the resulting sand-grain equivalent roughness height is k_s = 0.131 mm. Using the same mean momentum integral approach the estimation from Equation 10 yields $\%\Delta\bar{C}_f$ = 21.0% at cruise speed and 30.1% at full speed.

Table 4 summarises the percentage change in average skin friction coefficient $\%\Delta\bar{C}_f$ between the rough hull and hydrodynamically smooth wall for the Ro - Ro ferry at cruise and full-speed from experiment and various empirical estimation techniques. For the current roughness topography, the estimation methods of Chan et al. (2015) and Forooghi et al. (2017), are around 4.5%-5% higher than the experiment result while the

Townsin approximation produces 6%-7% lower than the experiment results. The Townsin approach produces slightly larger errors, which is likely related to the implicit assumption that k_s can be related to a single topographical height parameter (AHR). For further discussions regarding drag prediction techniques due to roughness, see Chung et al. (2021).

Method	$\%\Delta\bar{C}_f$ at cruise speed (4 m/s)	$\%\Delta\bar{C}_f$ at full speed (8 m/s)
Experiment	16.4%	25.2%
Townsin estimation	10.75%	18.35%
Chan et al (2015)	21.1%	30.1%
Forooghi et al (2017)	21.0%	30.1%

Table 4 : Comparison of full-scale hull roughness penalty for a typical Ro - Ro ferry, between experiment and various empirical estimation method.

Conclusions

An investigation into the influence of ship hull surface roughness topography from a cleaned and newly-painted ship-hull is discussed. Particular attention is given to the experimental technique (this includes scanning, scaling, and replication) and estimation of the drag penalty on full-scale ships. Here, comprehensive and carefully conducted turbulent boundary layer experiments via hot-wire anemometry permit us to obtain several important parameters, namely: skin friction velocity U_τ, the Hama roughness function ΔU^+, and equivalent sand-grain roughness height k_s. The velocity profile shift ΔU^+ as a function of viscous scaled equivalent sand-grain roughness height shows that the surface exhibits fully rough conditions even from a low $k_s^+ (\approx 10)$. The resulting equivalent sand-grain roughness height for this recently cleaned and painted ship hull is $\boldsymbol{k_s}$ **= 0. 101 mm**, which is higher than that reported for the typical "as applied" anti-fouling coatings (k_s = 0.03 mm) by Schultz (2007). This result is much closer to "deteriorated coating or light slime" that is typically associated with $k_S \approx 0.1$ mm. This discrepancy is possibly caused by the underlying hull roughness due to repeated cleaning (which often involves scraping, sand-blasting, and water blasting) and sub-optimal quality of anti-fouling paint application. Despite careful experiment and analysis, the authors would like to re-iterate that Schultz (2004) estimates that the experimental uncertainty in estimating ΔU^+ can varies between 6% -16%, this would lead to 10% - 27% uncertainty in estimating k_S.

By employing an integral boundary layer evolution method, it is estimated that this type of roughness will cause an increase in average coefficient of skin-friction $\%\Delta\bar{C}_f$ for a 71.82 m type Ro-Ro Ferry (with L.W.L = 68.46 m) at cruise speed of approximately 16.4%, rising to approximately 25.2% at full speed. Note however, the challenges in

predicting k_s would lead to around 7% - 10% uncertainty in the average skin friction coefficient $\overline{C_f}$. Hence cautions need to be taken when employing this experiment technique.

This report also shows that a newly reported empirical estimation method by Chan et al. (2015) and Forooghi et al. (2017), may serve as a preliminary estimation, yielding an accuracy of around 4.5%-5% higher in predicted skin friction coefficient compared to the experiment result. The Townsin approximation shows 6%-7% lower in the estimated skin friction coefficient than the experiment results.

In terms of a percentage change in total hydrodynamic resistance $\%\Delta\bar{R}_T$, this experiment approximation equates to increases of 8.2% and 7.5% at cruise and full-speed conditions respectively. Hence this study shows that even a well maintained and recently cleaned baseline hull may already suffer from a substantial drag penalty.

Disclosure Statement

No potential conflict of interest was reported by the authors

Acknowledgements

The authors would like to thank the Australian Research Council and the Newton Fund for the support of this work.

B. Ganapathisubramani is grateful to EPSRC for their support through grant EP/P009638/1.

I K A P Utama acknowledges the support from the Ministry of Research, Technology and Higher Education of the Republic of Indonesia under the World Class Professor 2019 Grant scheme: T/42/D2.3/KK.04.05/2019.

The authors thank PT Dharma Lautan Utama for providing access to the Dharma Kencana IX ferry, Dr Marcus Tullberg of Hempel A/S for his assistance in obtaining the hull roughness imprint, and PT Biro Klasifikasi Indonesia for ensuring the safety of the research team.

This paper uses re-analysis data from Nugroho et al. (2021) and they are openly available from the University of Southampton repository at https://doi.org/10.5258/SOTON/D1559.

References

Bandyopadhyay PR. 1987. Rough-wall turbulent boundary layers in the transition regime. J Fluid Mech. 180: 231–266.

Chan L, MacDonald M, Chung D, Hutchins N, Ooi A. 2015. A systematic investigation of roughness height and wavelength in turbulent pipe flow in the transitionally rough regime. J Fluid Mech, 771:743–777.

Chung D, Hutchins N, Schultz MP, Flack KA. 2021. Predicting the drag of rough surfaces. Annu Rev. Fluid Mech. 53: 439-471.
Clauser FH. 1954. Turbulent boundary layers in adverse pressure gradients. J Aeronaut Sci. 21:91–108.
Clauser FH. 1956. The turbulent boundary layers. Adv Appl Mech. 4, 1–151.
Cobert JJ, Fisbeck PS, Pandis SN. 1999. Global nitrogen and sulfur inventories for oceangoing ships. J Geophys Res. 104(D3): 3475 – 3470.
Colebrook, CF & White CM. 1937. Experiments with fluid friction in roughened pipes. Phil Trans R Soc. London, Ser. A. 16: 367–381.
Furuya Y, Miyata M, Fujita H. 1976. Turbulent boundary layer and flow resistance on plates roughened by wires. J Fluids Eng. 98(4): 653 – 643.
Flack KA, Schultz MP, Shapiro T A. 2005. Experimental support for Townsend's Reynolds number similarity hypothesis on rough wall. Phys Fluids. 17, 035102.
Flack KA, Schultz MP, Connelly JS. 2007. Examination of a critical roughness height for outer layer similarity. Phys Fluids. 19, 095104
Flack KA, Schultz P. 2010. Review of hydraulic roughness scales in the fully rough regime. J Fluids Eng. 132, 041203.
Flack K A, Schultz MP, Barros JM, Kim YC. 2016. Skin-friction behavior in the transitionally-rough regime. Int J Heat Fluid Flow. 61: 21-30.
Forooghi P, Stroh A, Magagnato F, Jakirlić S, Frohnapfel B. 2017. Toward a universal roughness correlation. J Fluids Eng. 139 (12): 121201
Granville PS. 1958. The frictional resistance and turbulent boundary layer of rough plates, Technical Report 1024. Navy Department.
Grigson C. 1985. The drag at ship scale of planes having any quality of roughness. J Ship Res 29(2): 94–104.
Grigson C. 1987. The full-scale viscous drag of actual ship surfaces and the effect of quality roughness on predicted power. J Ship Res. 31(3): 189–206.
Grigson C. 1992. Drag losses of new ships caused by hull finish. J Ship Res 36(2): 182–196.
Hama FR. 1954. Boundary-layer characteristics for smooth and rough surfaces. Trans Soc Nav Archit Mar Engrs. 62: 333–358.
Holtrop JA. 1977. Statistical analysis of performance test results. International Shipbuilding Progress. 24(270): 23–28.
Holtrop JA. 1984. Statistical re-analysis of resistance and propulsion data. International Shipbuilding Progress. 31: 272–276.
Holtrop J, Mennen GGJ. 1978. A statistical power prediction method. International Shipbuilding Progress. 25(290): 253–256.
Holtrop J, Mennen GGJ. 1982. An approximate power prediction method. International Shipbuilding Progress. 29(335): 166–170.
Hutchins N, Nickels TB, Marusic I, Chong MS. 2009. Hot-wire spatial resolution issues in wall-bounded turbulence. J Fluid Mech. 635: 103–136.
Hutchins N, Monty JP, Ganapathisubramani B, Nugroho B, Utama IKAP. (2016) Turbulent boundary layers developing over rough surfaces: from the laboratory to full-scale systems. 20th Australasian Fluid Mechanics Conference (AFMC). Perth, Australia.

ITTC. 2014. Recommended Procedures and Guidelines - 1978 ITTC performance prediction method 7.5-02-03-01.4 (Revision 03).
Jelly T, Busse A. 2018. Reynolds and dispersive shear stress contributions above highly skewed roughness. J Fluid Mech. 852: 710-724
Jimenez J. 2004. Turbulent flows over rough walls. Annu Rev Fluid Mech. 36: 173–196.
Kodama Y, Kakugawa A, Takahashi T, Kawashima H. 2000. Experimental study on microbubbles and their applicability to ships for skin friction reduction. Int J Heat Fluid Flow. 21: 582–588.
Lackenby H. 1962. Resistance of ships, with special reference to skin friction and hull surface condition. Proc Inst Mech Eng. 176: 981 – 1014.
Ligrani P M, Bradshaw P. 1987. Spatial resolution and measurement of turbulence in the viscous sublayer using subminiature hot-wires probes. Exp Fluids. 5: 407–417.
Marusic I, Monty JP, Hultmark M, Smits AJ, 2013. On the logarithmic region in wall turbulence. J Fluid Mech. 716 (R3): 1–11.
Marusic I, Chauhan KA, Kulandaivelu V, Hutchins N. 2015. Evolution of zero-pressure-gradient boundary layers from different tripping conditions. J Fluid Mech. 783: 379 – 411.
Marusic I, Chauhan KA, Kulandaivelu V, Hutchins N. 2016. Study of the streamwise evolution of turbulent boundary layers to high Reynolds numbers. Whither
Turbulence and Big Data in the 21st Century? pp. 47–560.
Molland AF, Turnock SR, Hudson DA, Utama IKAP. (2014) Reducing ship emissions: a review of potential practical improvements in the propulsive efficiency of future ships. Transactions of Royal Institution of Naval Architects Part A. 156: 175-188
Morrill-Winter C, Squire DT, Klewicki JC, Hutchins N, Schultz MP, Marusic I. 2017 Reynolds number and roughness effects on turbulent stresses in sandpaper roughness boundary layers. Phys Rev Fluids. 2, 054608.
Monty JP, Allen JJ, Lien K, Chong MS. 2011. Modification of the large-scale features of high Reynolds number wall turbulence by passive surface obtrusions. Exp Fluids. 51: 1755–1763.
Monty JP, Dogan E, Hanson R, Scardion AJ, Ganapathisubramani G, Hutchins N. 2016. An assessment of the ship drag penalty arising from light calcareous tubeworm fouling. Biofouling. 32(4): 451–464.
Nikuradse J. 1933 Stromungsgesetze in rauhen rohren. VDI-Forsch 361.
Nugroho B, Hutchins N, Monty JP. 2013. Large-scale spanwise periodicity in a turbulent boundary layer induced by highly ordered and directional surface roughness.
Int. J. Heat Fluid Flow. 41: 90– 102.
Nugroho B, Gnanamanickam EP, Kevin, Monty JP, Hutchins N. 2014. Roll-modes generated in turbulent boundary layers with passive surface modifications. AIAA paper.
Nugroho B, Baidya B, Nurrohman MN, Yusim AK, Prasetyo FA, Yusuf M, Suastika I K, Utama IKAP, Monty JP, Hutchins N, Ganapathisubramani B. 2017. In-situ turbulent boundary layer measurements over freshly cleaned ship-hull under steady cruising. Royal Institution of Naval Architects (RINA) Conference, International Conference on Ship and Offshore Technology (ICSOT). Jakarta, Indonesia.

Nugroho B, Utama IKAP, Monty J P, Hutchins N, Ganapathisubramani B. (2018) The influence of in-plane roughness wavelength relative to the boundary layer thickness. 12th International ERCOFTAC Symposium on Engineering Turbulence Modelling and Measurements (ETMM). Montpellier, France

Nugroho B, Monty JP , Utama IKAP, Ganapathisubramani B, and Hutchins, N (2021) Non k-type behaviour of roughness when1 in-plane wavelength approaches the boundary layer thickness. J Fluid Mech. 911:A1

Perry AE, Joubert PN. 1963. Rough-wall boundary layers in adverse pressure gradients. J Fluid Mech. 17: 193–211.

Perry AE, Schofield WH, Joubert PN. 1969. Rough wall turbulent boundary layers. J Fluid Mech. 37: 383–413.

Perry AE, Morrison GL, 1971. A study of the constant temperature hot-wire anemometer. J Fluid Mech. 47: 577–599.

Perry AE. 1982. Hot-wire anemometry. Oxford University Press, Oxford UK.

Perry AE, Li JD. 1990. Experimental support for the attached-eddy hypothesis in zero pressure-gradient turbulent boundary layers. J Fluid Mech. 218: 405–438.

Prandtl L, Schlichting H. 1955. The resistance law for rough plates. Technical Report 258. Navy Dept. Translated by P. Granville.

Pullin D I, Hutchins N, Chung D, 2017. Turbulent flow over a long flat plate with uniform roughness. Phys Rev Fluids 2, 082601(R).

Ramani A, Nugroho B, Monty JP, Hutchins N, Busse A, Jelly TO. (2020) The Effect of Anisotropic Surface Roughness on Turbulent Boundary-Layer Flow. 22nd Australasian Fluid Mechanics Conference (AFMC). Brisbane, Australia.

Schultz MP. 2002. The relationship between frictional resistance and rough-ness for surfaces smoothed by sanding. J Fluids Eng. 124: 492–499.

Schultz MP. 2004. Frictional resistance of antifouling coating systems. J Fluids Eng. 126: 1039–1047.

Schultz MP. 2007. Effects of coating roughness and biofouling on ship resistance and powering. Biofouling. 23:331–341.

Schultz MP, Bendick JA, Holm ER, Hertel WM . 2011.Economic impact of biofouling on a naval surface ship. Biofouling. 27:87–98.

Schultz MP, Flack KA. 2005. Outer layer similarity in fully rough turbulent boundary layers. Exp Fluids. 38: 328 – 340.

Schultz MP, Flack KA. 2007. The rough-wall turbulent boundary layer from the hydraulically smooth to the fully rough regime. J Fluid Mech. 580: 381–405.

Schultz P, Walker J , Steppe C N, Flack KA, 2015. Impact of diatomaceous biofilms on the frictional drag of fouling-release coatings. Biofouling. 31: 759–773.

Shockling MA, Allen JJ, Smits AJ. 2006. Roughness effects in turbulent pipe flow. J Fluid Mech. 564: 267–285.

Squire DT, Morrill-Winter C, Hutchins N, Marusic I, Schultz MP Klewicki JC. 2016a. Smooth- and rough-wall boundary layer structure from high spatial range particle image velocimetry. Phy Rev Fluids. 1, 064402.

Squire DT, Morrill-Winter C, Hutchins N, Schultz MP, Klewicki JC, Marusic I. 2016b Comparison of turbulent boundary layers over smooth and rough surfaces up to high reynolds numbers. J Fluid Mech. 795: 210–240.
Talluru KM, Kulandaivelu V, Hutchins N, Marusic, I 2014. A calibration technique to correct sensor drift issues in hot-wire anemometry. Mes Sci Tech. 25, 105304.
Townsend AA.1976. The structure of turbulent shear flow, 2nd ed. Cambridge University Press.
Thakkar M, Busse A, Sandham N, (2018). Direct numerical simulation of turbulent channel flow over a surrogate for Nikuradse-type roughness. J. Fluid Mech. 837, R1.
Townsin RL, Byrne D, Milne A, Svensen T. 1980. Speed, power and roughness: the economics of outer bottom maintenance. Nav Archit. 459–483.
Townsin RL, Byrne D, Svensen TE. Milne A. 1981. Estimating the techical and economic penalties of hull and propeller roughness. Trans. Soc Nav Archit Mar Engrs. 89: 295–318.
Townsin RL, 2003. The ship hull fouling penalty. Biofouling. 19: 9–15.
Winebrake JJ, Corbett J J, Green E H, Lauer A, Erying V. 2009. Mitigating the health impacts of pollution from oceangoing shipping: An assessment of low-sulfur fuel mandates. Environ Sci Technol. 43 (13): 4776 – 4782.
Wu Y, Christensen KT. 2007. Outer-layer similarity in the presence of a practical rough wall topography. Phys Fluids. 19, 085108.